

PAPER

CrossMark
click for updatesCite this: *RSC Adv.*, 2016, 6, 19298

Decontamination of methylene blue from aqueous solution by magnetic chitosan lignosulfonate grafted with graphene oxide: effects of environmental conditions and surfactant

Wei Zeng,^{ab} Yun-guo Liu,^{*ab} Xin-jiang Hu,^c Shao-bo Liu,^{de} Guang-ming Zeng,^{ab} Bo-hong Zheng,^d Lu-hua Jiang,^{ab} Fang-ying Guo,^{ab} Yang Ding^{ab} and Yan Xu^{ab}

In this study, magnetic chitosan lignosulfonate grafted with graphene oxide (MCLS/GO) as an innovative adsorbent was prepared successfully through a hydrothermal reaction. The adsorbent was also characterized using SEM, XRD, VSM, FTIR, XPS, and zeta-potential. The effects of pH, ionic strength, temperature and SDBS (sodium dodecylbenzene sulfonate) on the adsorption behavior of MB (methylene blue) by the MCLS/GO were investigated. The results indicate that MB removal is found to be more effective at a higher pH value and temperature. The adsorption process could be affected by ionic strength, particularly at a higher concentration. Isotherm and kinetics were well-fitted by a Langmuir isotherm model and pseudo-second-order model, respectively. In addition, the presence of SDBS had a positive effect on MB adsorption onto MCLS/GO. An intra-particle diffusion model indicates that both film diffusion and intra-particle diffusion were the rate-controlling processes. Thermodynamic analysis showed that the adsorption reaction was an endothermic and spontaneous process. The adsorption mechanism was proposed to be electrostatic attraction, π - π stacking interaction and hydrogen bonding via FTIR analysis. In conclusion, this study implies that MCLS/GO nanoparticles could be conveniently separated from a water body by an external magnet and utilized as an efficient adsorbent for environment purification.

Received 24th December 2015

Accepted 25th January 2016

DOI: 10.1039/c5ra27657h

www.rsc.org/advances

1. Introduction

Dyestuffs are widely utilized in dye synthesis, textile, electroplating, pharmaceuticals and cosmetics, and are serious contaminants due to their toxicity and coloration. Particularly, the aromatic structure of dyes could be difficult to remove or eliminate owing to their low biodegradability and stable structure toward biological and chemical treatment.¹ Various biological, physical, and chemical technologies have been applied for removing dyes such as microbial degradation, adsorption, coagulation, oxidation degradation and so on.²⁻⁵ Among these methods, adsorption has an upper hand over the

aforementioned processes due to its merits of simplicity, high efficiency, low energy requirements and economic feasibility.^{6,7} Heretofore, many materials, such as activated carbon,⁸ carbon nanotubes⁹ and biochar,¹⁰ have been extensively investigated as adsorbents for potential environmental applications to remove dyestuffs. In recent years, graphene has emerged as an adsorbent material, and has advantages in adsorption due to its unique physical and chemical properties, such as fast electron transfer, large surface area and chemical stability.¹¹

Graphene oxide (GO), as a precursor of graphene, not only inherits the merits of graphene, but also contains an amount of oxygen-containing functional groups, such as -COOH, -OH and C-O-C. These groups could be used as anchoring sites for contaminant occupation, which offers great promise for the removal and recovery of contaminants from aqueous solutions. However, GO is difficult to separate due to its hydrophilic nature,¹² which might severely hinder its practical application. Magnetic fluids have the capability to treat large amounts of wastewater within a short time and can be conveniently separated from wastewater. However, grafting ferrites directly to GO might greatly reduce the adsorption capacity due to the loss of adsorption sites. Therefore, it is necessary to find a better way to guarantee the adsorption capacity of GO and meet the requirement of easy separation.

^aCollege of Environmental Science and Engineering, Hunan University, Changsha 410082, P. R. China. E-mail: zw769873763@126.com; Fax: +86 731 88822829; Tel: +86 731 88649208

^bKey Laboratory of Environmental Biology and Pollution Control (Hunan University), Ministry of Education, Changsha 410082, P. R. China

^cCollege of Natural Resources and Environment, South China Agricultural University, Guangzhou 510642, P. R. China

^dSchool of Architecture and Art Central South University, Central South University, Changsha 410082, P. R. China

^eSchool of Metallurgy and Environment Central South University, Central South University, Changsha 410082, P. R. China

Chitosan, an abundant, renewable, biodegradable and non-toxic biomaterial, has two types of main reactive functional groups which are hydroxyl and amino. It is a very promising starting material for sequestering hazardous dyes,¹³ heavy metals¹⁴ and so on, but it is unstable in an aqueous environment. Coating chitosan with magnetic fluids to expand its function has been confirmed to improve its surface area by adding more adsorption sites and reducing the required dosage for the adsorption of dyes.¹⁵ LS (lignosulfonate) is a by-product from the pulp processing industry. It is a highly water-soluble polysulfonic product composed of functionalized phenylpropane units connected through alkyl and aryl ether linkages¹⁶ and has a large amount of functional groups. So far, LS, as an adsorbent modified material, has been scarcely investigated. In this work, magnetic chitosan–lignosulfonate (MCLS) was firstly synthesized through a hydrothermal method. The principle is based on the electrostatic interactions attributed to the $-\text{NH}_3^+$ from chitosan and $-\text{SO}_3^-$ of lignosulfonate which form a floccule and bond together by using glutaraldehyde as a cross-linker. Lastly, MCLS/GO was prepared *via* a reaction in which the carboxyl group of GO chemically combines with the amine group of magnetic chitosan–lignosulfonate. The final composite remarkably enhances the stability of GO in solution, could be easily separated, and is recoverable using an external magnet.

In this study, a renewable material MCLS/GO was prepared and characterized (SEM, XRD, VSM, FTIR, XPS and zeta-potential) to investigate its adsorption behavior for MB. Batch experiments were carried out to study the effects of pH, initial MB concentration, contact time, ionic strength, and temperature on MB adsorption. SDBS, a kind of anionic surfactant, has a great possibility to co-exist with MB in a mixed contaminant system. Thus, the effects of SDBS on MB adsorption capacity were also investigated. Adsorption kinetics, isotherm, and thermodynamics were simulated to study the adsorption properties for MB by MCLS/GO. In addition, the desorption capacity and proposed adsorption mechanism were also elucidated.

2. Materials and methods

2.1 Materials

Graphite powder (particle size $\leq 30 \mu\text{m}$) was supplied by Tianjin Hengxin Chemical Preparation Co., Ltd., China. Chitosan (90% acetylation degree) was purchased from Sinopharm Chemical Reagent Co. Ltd., Shanghai, China. Sodium lignosulfonate was provided by Shanghai Maklin Biochemical Co., Ltd. Methylene blue trihydrate ($\text{C}_{16}\text{H}_{18}\text{ClN}_3\text{S}\cdot 3\text{H}_2\text{O}$, 99% in purity) was obtained from Municipality Kemi'ou Chemical Reagent Co. Ltd., Tianjin. All other chemicals employed in the experiments were purchased at analytical reagent grade and used without any further purification. In addition, all the solutions were prepared using high purity water ($18.25 \text{ M}\Omega \text{ cm}^{-1}$) from a Millipore Milli-Q water purification system. A stock solution (1000 mg L^{-1}) of MB was prepared by dissolving 1.169 g of $\text{MB}\cdot 3\text{H}_2\text{O}$ in 1000 mL of distilled water. The different concentrations of solution used

in the various experiments were obtained by diluting the stock solution.

2.2 Preparation of MCLS/GO

GO was prepared from natural graphite by a modified Hummers method.¹⁷ Briefly, graphite was firstly pre-oxidized by H_2SO_4 (98%), $\text{K}_2\text{S}_2\text{O}_8$, and P_2O_5 , and stirred at 80°C for 4.5 h. Next, H_2SO_4 (98%), KMnO_4 , and NaNO_3 were used to oxidize the pre-oxidized graphite powders. After that, 30% H_2O_2 was added to remove surplus MnO_4^- . Then, the products were rinsed by HCl (10%) and Milli-Q water until the pH was neutral. The resulting solution was sonicated for 2 h, and a GO dispersion was obtained.

Magnetic fluids was prepared as follows:¹⁸ An Fe^{2+} and Fe^{3+} (2 : 3) solution was added to a beaker with stirring at 55°C and then NaOH solution was added dropwise until the pH reached 9.0, with constant stirring, for 10 min. Next, the temperature of the reaction vessel was raised to 65°C and 0.8 mL of Tween 80 was added into the mixture with stirring for 30 min, and then the pH value was adjusted to 7.0. After that, the sol was washed with Milli-Q water three times and was dispersed in an ultrasonic device for 40 min. Finally, the solution was diluted to obtain the magnetic fluid (40 g L^{-1}).

MCLS/GO was synthesized through a hydrothermal reaction. 0.03 M EDC and 0.06 M NHS solutions were added to the GO dispersion with continuous stirring for 1 h in order to activate the carboxyl groups of GO.¹⁹ Chitosan (1.0 g) was added into 50 mL of 1% acetic solution with stirring at 50°C until absolutely dissolved, then 10 mL of magnetic fluid was added slowly into the above solution with constant stirring for 30 min, and the pH value was adjusted to 6.0. Next, sodium lignosulfonate solution (20 g L^{-1}) (adjusted pH = 6.0) was added drop by drop until the emergence of a floccule, and then glutaraldehyde (1% v/v) was added into the mixed system as a crosslinker with constant stirring for 2 h. Then, the mixture was added into the activated GO dispersion, and stirred continuously for 2 h in a water bath at 60°C . After that, glutaraldehyde (1% v/v) was then injected into the reaction system and reacted for 2 h. Next, NaOH solution was added dropwise into the mixtures until the pH value reached 8.0–10.0. Lastly, the resulting product was washed repeatedly until the pH was about neutral, then was dried at 50°C and sieved through a 150 mesh screen. A scheme of the preparation of MCLS/GO is shown in Fig. 1.

2.3 Characterization

The morphology of MCLS/GO was characterized using scanning electron microscopy (SEM) (JEOL JSM-6700, Japan). The X-ray diffraction (XRD) patterns of GO, Fe_3O_4 and MCLS/GO composite were obtained using an X-ray diffractometer (Rigaku D/max-2500, Japan) with $\text{CuK}\alpha$ radiation. Magnetization measurements were performed using a vibrating sample magnetometer (VSM) (MPMS XL-7, America). Fourier transform infrared spectroscopy (FTIR) of the samples was performed using a spectrophotometer (Nicolet, Magna 550 spectrometer). The elements of the samples were confirmed using an ESCALAB 250 Xi X-ray Photoelectron Spectrometer (XPS) (Thermo Fisher,

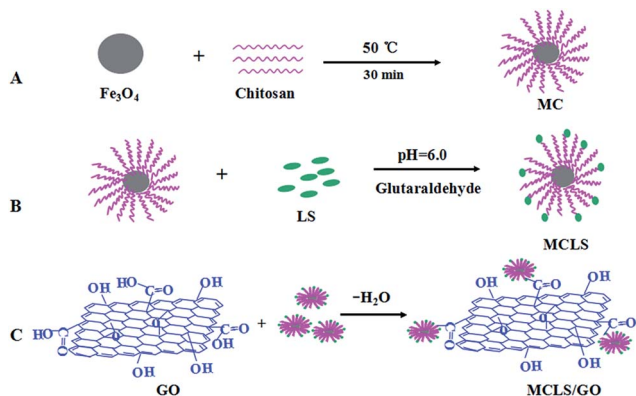


Fig. 1 Schematic depiction of the formation of MCLS and MCLS/GO.

USA). The zeta-potential of MCLS/GO was obtained using an electroacoustic spectrometer (ZEN3600 Zetasizer UK) under a solution pH varying from 2.0 to 11.0.

2.4 Sorption experiment

All batch sorption experiments were carried out in 50 mL Erlenmeyer flasks containing 20 mL of MB solution and 10 mg of adsorbent in an incubator shaker with a shaking speed of 160 rpm. For each group, the initial pH of the solution was adjusted by adding an appropriate dose of NaOH and HCl. Next, 10 mg of adsorbent was poured into the system and then shaken at 30 ± 0.2 °C for a specified time. The dispersion was drawn and separated immediately by the aid of an external magnet after adsorption. The residual concentration of MB was determined using a UV spectrophotometer (Pgeneral T6, Beijing, China) at 665 nm. Adsorption efficiency E (%) and the amount of MB adsorbed q_e (mg g^{-1}) were calculated using the following equations:

$$E = (C_0 - C_e) \times 100/C_0 \quad (1)$$

$$q_e = (C_0 - C_e) \times V/m \quad (2)$$

where C_0 (mg L^{-1}) and C_e (mg L^{-1}) are the initial and equilibrium concentrations of MB, V (L) stands for the volume of solution, and m (g) is the mass of adsorbent.

2.5 Desorption experiment

Desorption of MB and regeneration of MCLS/GO composites was carried out with 0.5 mol L^{-1} HCl as a stripping reagent. In detail, the experiment was conducted as follows: the adsorbent was firstly used to remove MB (400 mg L^{-1}) and collected. Next, the collected adsorbent was added into 20 mL of 0.5 mol L^{-1} HCl solution and shaken at 160 rpm for a specified time at a temperature of 30 ± 0.2 °C. Finally, the residual contaminant-laden MCLS/GO was withdrawn by an external magnet, washed repeatedly until the pH was about neutral, and then collected for reuse.

3. Results and discussion

3.1 Characterization

Fig. 2 shows an SEM micrograph of GO and MCLS/GO. In Fig. 2a, the large thickness, smooth surface and wrinkled edge typical of an SEM image of GO are present. After grafting with MCLS to form the final adsorbent (Fig. 2b), there is a clear change visible, in that MCLS/GO has a much rougher surface, which might be because MCLS/GO is immobilized on the surface of GO layers with a high density. Obviously, the rough morphology of MCLS/GO could present a higher surface area, which might be beneficial for attracting more target contaminants.

The XRD patterns of pure GO, magnetic fluids, and MCLS/GO are presented in Fig. 3a. As shown in the figure, for GO, a well-defined peak at $2\theta = 10.8^\circ$ is observed, indicating the presence of abundant oxygen-functional groups on both sides of the GO sheets. These results correspond to the previous study.²⁰ Six characteristic peaks at $2\theta = 30.1^\circ, 35.5^\circ, 43.3^\circ, 53.4^\circ,$

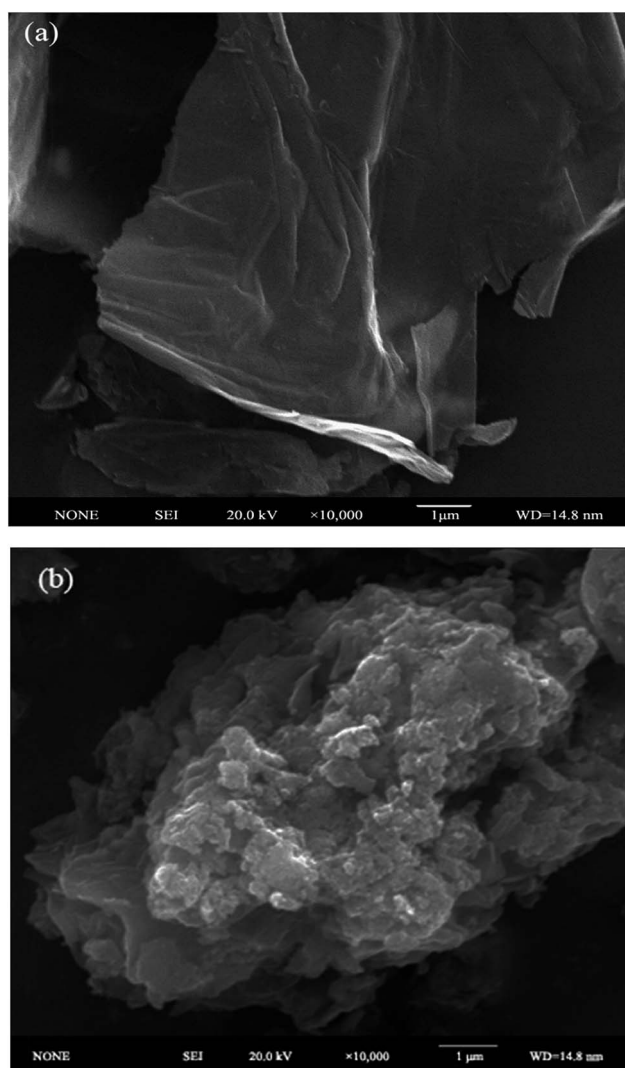


Fig. 2 SEM images of (a) GO and (b) MCLS/GO.

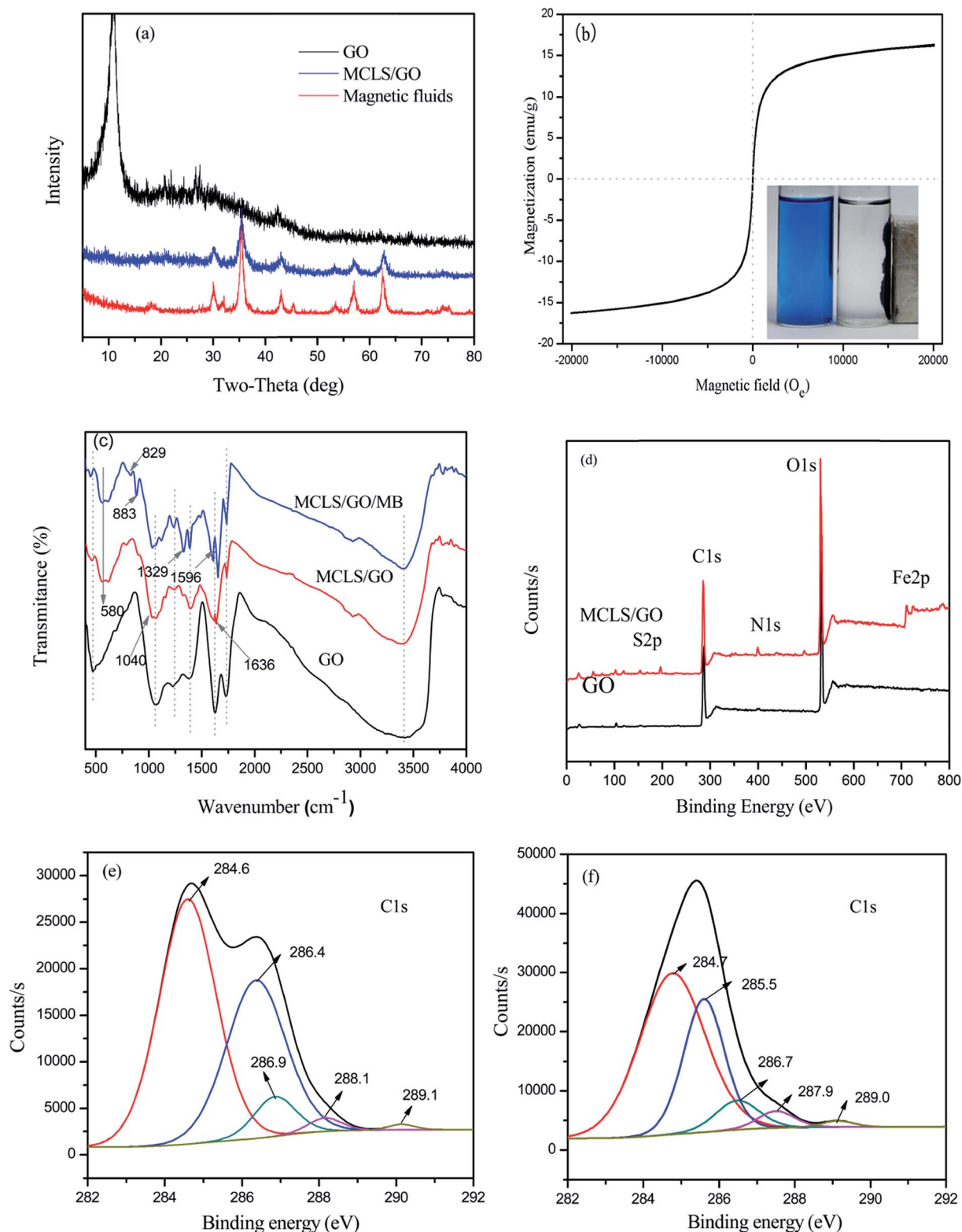


Fig. 3 XRD patterns (a) of GO, magnetic fluids, and MCLs/GO; magnetization curve (b) of MCLs/GO at room temperature; FTIR spectra (c) of GO and MCLs/GO before and after MB adsorption; XPS full scans (d) of GO and MCLs/GO; C1s XPS spectra of (e) GO and (f) MCLs/GO.

57.2° and 62.5° are observed clearly in the XRD pattern of magnetic fluids. These peaks are consistent with the standard XRD data for cubic phase Fe_3O_4 with a face-centered cubic (fcc)

structure.²¹ There are no diffracted signals for GO sheets in MCLs/GO compared with pure GO, which might be because the strong signals of Fe_3O_4 tend to overwhelm the relatively weak

carbon peaks. Besides that, it was hard to find any difference in the XRD patterns of MCLS/GO and magnetic fluids, demonstrating that the synthesis process did not change the crystalline phase of Fe_3O_4 .

The room-temperature magnetization hysteresis curve is shown in Fig. 3b, and it presents a typical feature (an S-like loop). Zero retentivity and coercivity in the magnetization loop were observed, which indicates super-magnetization of the particles.²² It is noteworthy that the saturation magnetization of MCLS/GO is 16.3 emu g^{-1} which is sufficient for meeting the requirement of solid-liquid separation by an external magnet. The inset in Fig. 3b testifies the favorable separation characteristics and demonstrates the feasibility of MCLS/GO for removing MB from aqueous solution.

GO and MCLS/GO were characterized by FTIR in the range of 4000 to 400 cm^{-1} , and the results are shown in Fig. 3c. Several characteristic peaks of GO, such as C–O (472 cm^{-1}), C–O–C (1053 cm^{-1}), C–OH (1225 cm^{-1}), C=O (1402 and 1730 cm^{-1}), O–H (3408 cm^{-1}), and C=C (1624 cm^{-1}) were observed. As for chitosan, there are two characteristic bands centered at 1636 and 1578 cm^{-1} , which correspond to the C=O stretching vibration of –NHCO– (amide I) and the N–H bending of –NH₂, respectively.²³ However, for MCLS/GO, the –NH₂ characteristic peak has a lower value and the intensity of acetylated amino groups –NHCO– (amide I) shifted to a higher wavenumber. Thus, some of the –NH₂ groups in chitosan react with –COOH functional groups on the surface of GO, and further convert into –NHCO– groups. In addition, new bands emerging at 580 and 1040 cm^{-1} were observed, which were assigned to the Fe–O of Fe_3O_4 and S=O symmetric stretching of the –SO₃ groups on LS chains.²⁴ It might be that magnetic fluids and lignosulfonate were successfully introduced into the composites. Therefore, the information given by the FTIR spectra proves that MCLS/GO was prepared successfully. Additionally, the spectrum of MB-laden MCLS/GO is also displayed in Fig. 3c, and a detailed description of MCLS/GO/MB will be discussed in the following section concerning the adsorption mechanism.

The XPS spectra of GO and MCLS/GO are presented in Fig. 3d. The full scan spectrum of GO shows the C and O peaks at binding energies of 284.6 and 533.0 eV , respectively. Elemental analysis indicates that the ratio of C/O is 1.80 . There were three additional peaks, N (400.2 eV), S (169.2 eV) and Fe (711.4 eV) after modification, which may originate from chitosan, lignosulfonate, and magnetic fluids, respectively. The existence of N, S and Fe implies that the MCLS/GO was successfully prepared. For the MCLS/GO XPS spectrum, the peaks of C and O slightly shift to 284.7 and 533.6 eV , respectively. The C/O atomic ratio for MCLS/GO is 1.54 , indicating that there are more oxygen-containing functional groups in MCLS/GO compared with the pristine GO. These results correspond with the FTIR characteristics.

To further investigate the functional groups of GO and MCLS/GO, software was applied to analyze the C1s XPS spectra of GO (Fig. 3e) and MCLS/GO (Fig. 3f). For the C1s XPS spectrum of GO, five significant peaks centered at 284.6 , 286.4 , 286.9 , 288.1 and 289.1 eV were observed, which correspond to C=C/C–C, C–O, C–O–C, C=O, and –COOH, respectively. The C1s

spectrum of MCLS/GO can also be divided into five fitted curves at binding energies of about 284.7 , 285.5 , 286.7 , 287.9 and 289.0 eV , which are consistent with the carbon atoms in the C=C/C–C, C–N, C–O–C, –NHCO–, and –COOH species, respectively. The existence of –NHCO– adequately proves that GO and MCLS react with the –COOH groups on the surface of GO and the –NH₂ groups of chitosan.

3.2 Effect of pH

Solution pH value is one of the key factors that determines the adsorption capacity of an adsorbent. It can not only affect the degree of deprotonation and the speciation of surface functional groups on adsorbent, but also the state of the adsorbate.²⁵ The effect of pH on sorption experiments was investigated over a pH range from 2.0 to 11.0 at an initial MB concentration of 50 mg L^{-1} . From Fig. 4, the removal efficiency of MB increased quickly over the pH range 2.0 – 5.0 , and the tendency changed insignificantly over the pH range from 5.0 to 11.0 . The result corresponds with the zeta potential of MCLS/GO. The pH_{zpc} (point of zero charge) of MCLS/GO estimated by electroacoustic spectrometry was about 2.3 . When $\text{pH} < \text{pH}_{\text{zpc}}$, the surface of the adsorbent was positively charged due to protonation, which resulted in electrostatic repulsion between MCLS/GO and MB. Moreover, the existence of H^+ lead to great competition with MB for adsorption sites, further contributing to the relatively low adsorption efficiency. When the pH value was increased, the surface of adsorbent was negatively charged, and the electrostatic attractions between the MCLS/GO and the MB were strengthened.

3.3 Adsorption isotherm and the effect of surfactant concentration

In order to investigate the adsorption behavior between solid and liquid phase at equilibrium, a batch experiment was carried out with various initial concentrations (50 – 250 mg L^{-1}) at pH 10.0 . Simultaneously, the effect of surfactant (SDBS)

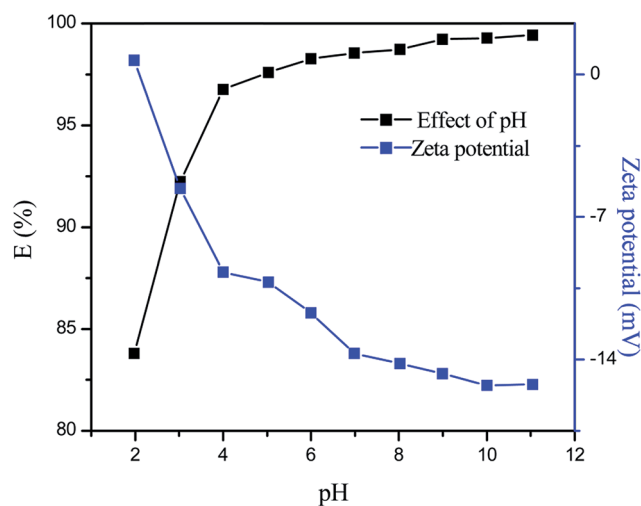


Fig. 4 Zeta-potential of MCLS/GO at different pH values and the effect of initial solution pH on MB adsorption.

concentration on maximum adsorption capacity was investigated by adding different concentrations (10, 50 and 100 mg L⁻¹) into the isotherm reaction system, and the results are presented in Fig. 5. The Langmuir and Freundlich isotherm models are the most common models to analyze the sorption equilibrium data. The Langmuir model is based on the assumption that the surface of the adsorbent has finite adsorption sites, and the adsorbate is adsorbed by homogeneous sites without mutual interaction. It is presented in the following eqn (3):

$$q_e = \frac{q_{\max} K_L C_e}{1 + K_L C_e} \quad (3)$$

where q_{\max} is the maximum adsorption at monolayer coverage (mg g⁻¹) and K_L is the Langmuir adsorption equilibrium constant (L mg⁻¹) reflecting the energy of adsorption. R_L , called the separation factor of equilibrium parameters, is used to determine the favorability of MB adsorption process, and is given according to eqn (4):²⁶

$$R_L = \frac{1}{1 + K_L C_0} \quad (4)$$

$0 < R_L < 1$, indicating that MB adsorbed onto MCLS/GO is favorable.

The Freundlich model is presented in the following form (eqn (5)).

$$q_e = K_F C_e^{1/n} \quad (5)$$

K_F (L mg⁻¹) and $1/n$ are the Freundlich characteristic constants, indicating adsorption capacity and adsorption intensity, respectively. If n is more than 1 and less than 10, the adsorption represents favorable adsorption conditions.²⁷

The isotherm parameters calculated from the two models are listed in Table 1. It can be obviously seen that the correlation coefficient (R^2) values of the Langmuir model are much better than the values of the Freundlich model. Therefore, the

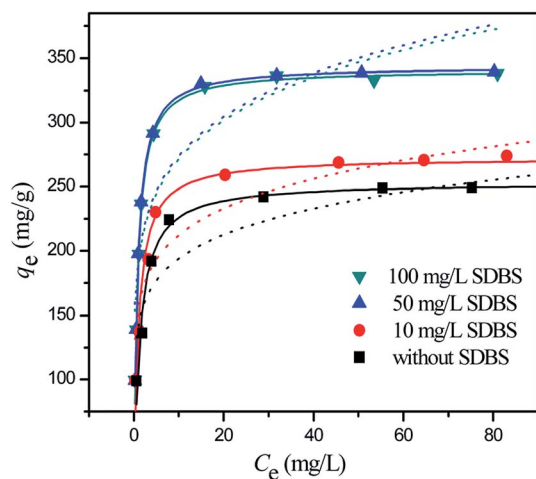


Fig. 5 Langmuir (solid) and Freundlich (dot) non-linear plots of the sorption isotherm for MB adsorption by MCLS/GO in the presence of different SDBS concentrations.

adsorption behavior was more suitable for the Langmuir model, indicating the homogeneous and monolayer adsorption of MB onto the adsorption sites. In addition, all the R_L values were between 0 and 1, which demonstrates that MCLS/GO is a favorable adsorbent to sequester MB from aqueous solution. Furthermore, it was clearly found that the q_{\max} and K_L of the Langmuir model increased when increasing the SDBS concentration from 0 mg L⁻¹ to 50 mg L⁻¹, and remained almost constant from 50 mg L⁻¹ to 100 mg L⁻¹, which could be because the interactions between MB and the active sites of the adsorbent were strengthened in the presence of SDBS. This might be due to the following: (1) the existence of SDBS improves the dispersion of nanoparticles which greatly enhances the possibility of combination between MB and MCLS/GO; (2) there are possible interactions attributed to the formation of (MB⁺)(SDB⁻) and (H⁺)(SDB⁻) complex compounds on the reactive sites on MCLS/GO surfaces,²⁸ which further lead to the modification of the surfaces and reduce electrostatic repulsion. However, SDBS begins to aggregate if the concentration is higher than the CMC (critical micelle concentration).²⁹ The complex compounds of (MB⁺)(SDB⁻) decrease with increasing SDBS concentration primarily due to the counterion binding of MB⁺ to any micelles. Thus, the adsorption capacity remains constant in the presence of 100 mg L⁻¹ SDBS. The maximum MB adsorption capacity of different adsorbents in the previous study are presented in Table 2. As seen in Table 2, the MCLS/GO has a higher adsorption capacity for MB than other materials reported in the literature.

3.4 Effect of contact time and adsorption kinetics

The effect of contact time on MB adsorption onto MCLS/GO was investigated at pH = 10.0 by varying the treatment time from 0 to 48 h. The adsorption behavior of MB onto MCLS/GO in the presence of 50 mg L⁻¹ SDBS was also investigated. It is noteworthy in Fig. 6a that the adsorption rate of MB uptake is very fast and the maximum adsorption capacity is obtained within the initial 3 h. Doubling MB concentration from 50 to 100 mg L⁻¹ leads to a doubling of adsorption capacity, indicating that there are extra adsorption sites for MB adsorption. The very fast adsorption rate during the initial 3 h could be attributed to a great number of functional groups on the MCLS/GO surface.

Adsorption kinetics was investigated using a pseudo-first-order model and pseudo-second-order model. The non-linearized equations of the pseudo-first-order and pseudo-second-order models can be described as follows:

$$\text{Non-linear pseudo-first-order : } q_t = q_{e,1} (1 - e^{-k_1 t}) \quad (6)$$

$$\text{Non-linear pseudo-second-order : } q_t = \frac{q_{e,2}^2 k_2 t}{1 + k_2 q_{e,2} t} \quad (7)$$

where q_t (mg g⁻¹) is the mass of MB adsorbed per gram at time t (min), $q_{e,1}$ and $q_{e,2}$ (mg g⁻¹) are the adsorption capacities calculated by pseudo-first-order and pseudo-second-order models, respectively, and k_1 (min⁻¹) and k_2 (g mg⁻¹ min⁻¹) are the adsorption rate constants of the pseudo-first-order and

Table 1 Constants and correlation coefficients of Langmuir and Freundlich models for MB adsorption onto MCLS/GO

	Langmuir			Freundlich		
	q_{\max} (mg g ⁻¹)	K_L (L mg ⁻¹)	R^2	K_F (L mg ⁻¹)	n	R^2
MB	253.533	0.824	0.9701	143.271	7.580	0.8197
MB + 10 mg L ⁻¹ SDBS	272.556	1.039	0.9385	155.152	7.386	0.8519
MB + 50 mg L ⁻¹ SDBS	343.902	1.357	0.9991	192.891	6.559	0.8085
MB + 100 mg L ⁻¹ SDBS	341.153	1.332	0.9911	191.595	6.596	0.8148

Table 2 Comparison of the maximum MB adsorption capacity with other adsorbents

Adsorbents	Adsorption capacity (mg g ⁻¹)	References
GNS/Fe ₃ O ₄	43.82	30
MCCGO	84.32	31
Graphene	153.85	32
MCGO	180.83	23
MCLS	81.40	This work
MCLS/GO	253.53	This work

pseudo-second-order models, respectively. h (mg g⁻¹ min⁻¹) is the initial MB adsorption rate and it is given by eqn (8):

$$h = k_2 q_{e,2}^2 \quad (8)$$

After being fitted by the two models, the calculated parameters are listed in Table 3. It can be seen that the pseudo-first-order model has relatively low correlation coefficients (R^2). Additionally, the q_e value calculated using this model was different with the experimental value. Therefore, MB adsorption onto MCLS/GO cannot be classified by this model. In contrast, the correlation coefficients (R^2) of the pseudo-second-order model were all extremely higher (greater than 0.900). Meanwhile, the experimental q_e values were in very good agreement with theoretical data. These facts suggest that the pseudo-second-order model adsorption mechanism was predominant.

From Table 3, it was obvious to find that the initial adsorption rates with 50 mg L⁻¹ SDBS were higher than in the system without SDBS, which might be explained by the existence of SDBS being beneficial for attracting more MB molecules. This corresponds with the results of isotherm investigation.

The pseudo-first-order and pseudo-second-order models can be used to analyze the possible adsorption behavior of MB onto MCLS/GO, but they could not integrally describe the process of MB transportation from aqueous solution to the surface of adsorbents. Thus, the introduced intra-particle diffusion model is necessary. The intra-particle diffusion model can be described by the following eqn (9).

$$q_t = k_p t^{0.5} + C \quad (9)$$

where k_p is the intra-particle diffusion model rate constant and C is a constant related to the thickness of the boundary layer. In general, the adsorption reaction includes four steps: (1) bulk diffusion, (2) film diffusion, (3) intra-particle diffusion, and (4) adsorption on the internal surface of the adsorbent.³³ As we all know, rate control is given by the slowest reaction process. However, bulk diffusion and adsorption onto the interior pore structure of the adsorbents are very fast, and the contact time can be ignored. So, the adsorption process is controlled by film diffusion or intra-particle diffusion.³⁴ The plot of q_t versus $t^{0.5}$ is shown in Fig. 6b and it was noticed that the adsorption process was not linear over the whole range of reaction time. The plot has been divided into three regions. The first stage with a large

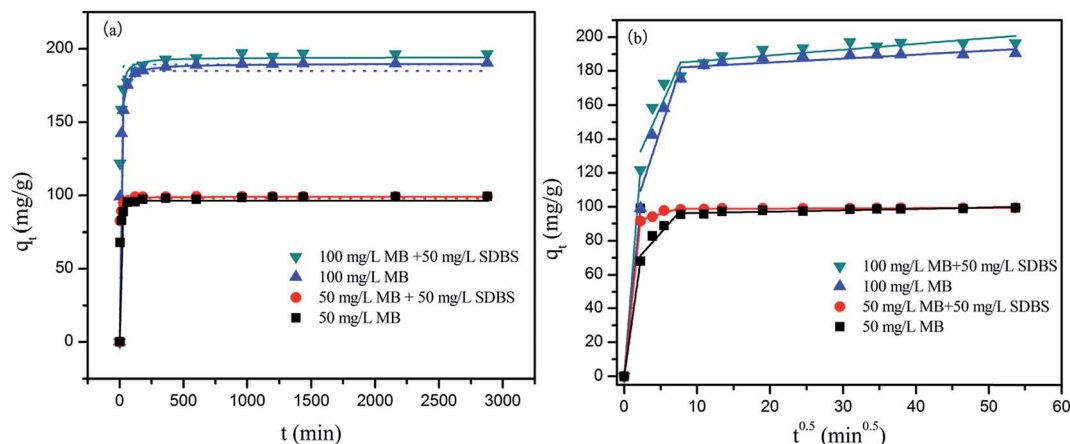


Fig. 6 Pseudo-first-order (dot) and pseudo-second-order (solid) non-linear plots (a) of adsorption kinetics for MB onto adsorbents at two different concentrations with and without 50 mg L⁻¹ SDBS, and (b) intra-particle diffusion kinetics.

Table 3 Pseudo-first-order and pseudo-second-order model parameters for MB adsorption by MCLS/GO

Concentration	Pseudo-first-order			Pseudo-second-order			<i>h</i> (mg g ⁻¹ min ⁻¹)	<i>q_{e,exp}</i> (mg g ⁻¹)
	<i>q_{e,1}</i> (mg g ⁻¹)	<i>k₁</i> × 10 (min ⁻¹)	<i>R</i> ²	<i>q_{e,2}</i> (mg g ⁻¹)	<i>k₂</i> × 10 ³ (g mg ⁻¹ min ⁻¹)	<i>R</i> ²		
50 mg L ⁻¹ MB	96.298	2.2195	0.7736	98.395	4.207	0.9832	40.731	99.370
50 mg L ⁻¹ MB + 50 mg L ⁻¹ SDBS	97.789	3.6551	0.6619	99.034	9.172	0.9463	89.956	99.208
100 mg L ⁻¹ MB	188.359	1.3678	0.9132	189.852	1.077	0.9951	38.819	190.300
100 mg L ⁻¹ MB + 50 mg L ⁻¹ SDBS	189.241	1.1788	0.7831	194.110	1.602	0.9737	60.361	196.500

slope represents the mass transferred from the boundary film to the external surface of MCLS/GO by film diffusion. The second phase was the gradual adsorption process, which shows that MB molecules migrate to the internal structure of the adsorbents by intra-particle diffusion. The last portion was an almost horizontal line, that indicates the adsorption–desorption equilibrium. Therefore, the intra-particle diffusion is not the only rate-limiting step, and MB adsorption onto MCLS/GO mainly involves film diffusion and intra-particle diffusion.

3.5 Effect of ionic strength

The effect of salt (NaCl) ionic strength on the sequestration of MB by MCLS/GO was investigated by adding various sodium chloride concentrations (0, 0.001, 0.005, 0.01, 0.05, 0.1, and 0.1 M) into the reaction system with 100 mg L⁻¹ initial MB concentration. The experimental results are presented in Fig. 7a. The presence of NaCl has scarcely any effect on MB adsorption at lower concentrations (0–0.1 M). However, there is a significant decline (from 192.564 to 157.200 mg g⁻¹) as NaCl concentration increases from 0.1 to 0.5 M. This phenomenon could be explained by the following two reasons. On the one hand, the existence of salts might screen the electrostatic interactions between MB cations and MCLS/GO due to competitive adsorption. But, on the other hand, the MB molecules could dissociate to MB⁺ due to the effect of salts, which would thus result in the enhancement of the electrostatic

attraction between MB cations and MCLS/GO.³⁵ However, when further increasing the NaCl concentration to 0.5 M, the latter could not integrally offset the negative effects, which led to a decline in adsorption capacity. This could be explained by the fact that the adsorbents can aggregate into together due to the enhancement of electrostatic repulsion, and more Na⁺ competes with MB when the concentration NaCl reached to 0.5 M, which further extremely reduces the uptake capacity of MCLS/GO for MB.³⁶

3.6 Thermodynamic studies

To further estimate the adsorption behavior of MB onto MCLS/GO, the effects of temperature on the adsorption process were studied. These experiments were conducted at a fixed initial MB concentration at three different temperatures of 303, 313 and 323 K. The thermodynamic parameters of Gibbs free energy (ΔG), entropy (ΔS), and enthalpy (ΔH) can be presented in the form of the following eqn:¹⁵

$$\ln \frac{q_e}{C_e} = \frac{-\Delta H}{RT} + \frac{\Delta S}{R} \quad (10)$$

$$\Delta G = \Delta H - T\Delta S \quad (11)$$

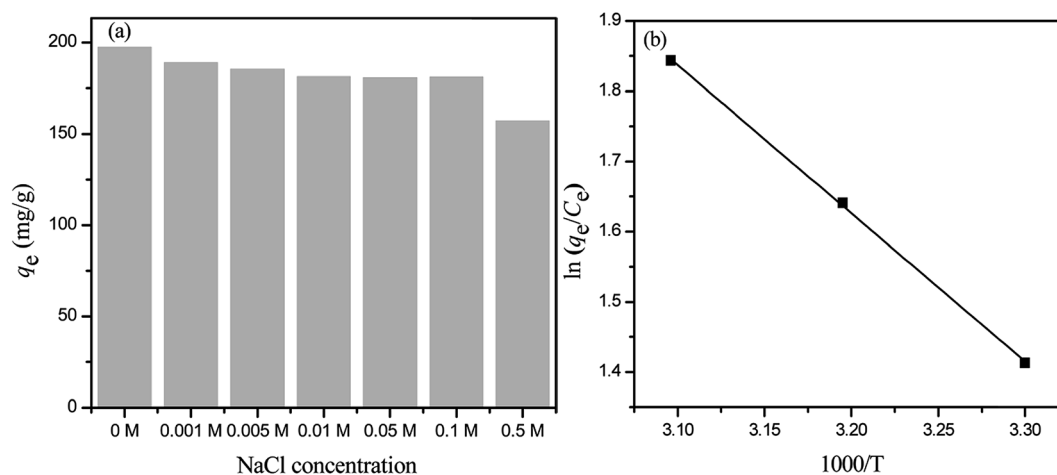


Fig. 7 Effect of ionic strength (a) (NaCl) on MB adsorption and a plot of $\ln(q_e/C_e)$ versus $1000/T$ (b) for estimation of the thermodynamic parameters of MB adsorption by MCLS/GO.

where T (K) is the absolute temperature in Kelvin, ΔS ($\text{kJ} (\text{K}^{-1} \text{mol}^{-1})$) is the entropy change, ΔH ($\text{kJ} \text{mol}^{-1}$) is the enthalpy change, and R ($8.314 \text{ J} (\text{mol}^{-1} \text{K}^{-1})$) is the universal gas constant. The values of ΔH and ΔS were obtained from the slope and intercept of the plot between $\ln(q_e/C_e)$ versus $1/T$ (Fig. 7b), respectively. The calculated thermodynamic parameters are presented in Table 4. The negative values of ΔG were found to decrease from -3.559 to $-4.951 \text{ kJ} \text{mol}^{-1}$ when the temperature increased from 303 to 323 K, indicating that MB adsorption was feasible and spontaneous. The positive values of ΔH ($17.562 \text{ kJ} \text{mol}^{-1}$) elucidate that the adsorption reaction was an endothermic process, and the positive ΔS ($69.719 \text{ kJ} (\text{K}^{-1} \text{mol}^{-1})$) further implies an increasing randomness at the solid/solution surface during adsorption.¹⁸

3.7 Desorption and reusability analysis

The feasibility of desorption and regeneration is an important parameter to assess reusability and economic value. In this study, 0.5 mol L^{-1} HCl was selected as stripping reagent to investigate desorption and reusability for 6 cycles, and the results are shown in Fig. 8. It was obvious to find that adsorption capacity decreased gradually within 3 cycles (from $192.564 \text{ mg g}^{-1}$ to $182.337 \text{ mg g}^{-1}$), but there was a dramatic drop in the subsequent cycles (from $155.235 \text{ mg g}^{-1}$ to $120.600 \text{ mg g}^{-1}$), indicating a relatively good reusability of MCLS/GO for MB sequestration. The decreasing adsorption capacity trend might be explained by the reduction in surface area, the blockage of pore volume, and the relatively less adsorption sites available.

3.8 Adsorption mechanism

The FTIR spectra of MCLS/GO and MCLS/GO/MB were used to investigate the adsorption mechanism (Fig. 3c). The characteristic peaks of MCLS/GO at 1240 and 3390 cm^{-1} , corresponding to the $-\text{OH}$ stretching vibration, slightly shifted to 1236 and 3396 cm^{-1} after adsorption. The peaks of nanoparticles at 1392 and 1736 cm^{-1} , corresponding to the carbonyl of the carboxyl group, migrated to 1386 and 1735 cm^{-1} , indicating that hydroxyl and carboxyl groups of MCLS/GO play a key role in the adsorption process. The surface of MCLS/GO was negatively charged due to the ionization of hydroxyl and carboxyl groups, which might be explained by electrostatic attractions between negatively charged oxygen-functional groups and positively charged MB being a significant adsorption mechanism. This was in accordance with the results of pH-dependent adsorption experiments. As for MB, there are three characteristic peaks at 826 , 880 , and 1589 cm^{-1} , ascribed to the $\text{C}=\text{C}$ stretching

Table 4 Thermodynamic analysis data for MB adsorption onto MCLS/GO

T (K)	ΔG ($\text{kJ} \text{mol}^{-1}$)	ΔS ($\text{kJ} (\text{K}^{-1} \text{mol}^{-1})$)	ΔH ($\text{kJ} \text{mol}^{-1}$)
303	-3.559	69.719	17.562
313	-4.270		
323	-4.951		

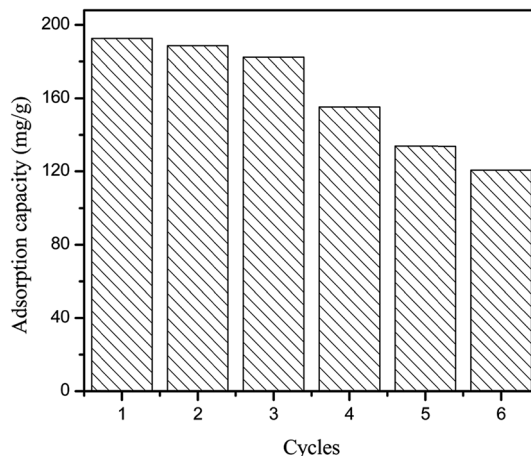


Fig. 8 Six consecutive adsorption–desorption cycles of MCLS/GO for MB removal.

vibrations of the aromatic ring. However, these peaks shifted to 829 , 883 , and 1596 cm^{-1} after MB was adsorbed by MCLS/GO. Besides, the characteristic band of MCLS/GO at 1616 cm^{-1} , corresponding to a $\text{C}=\text{C}$ stretching vibration, may overlap with the adsorption band at 1596 cm^{-1} . Each $\text{C}=\text{C}$ of the aromatic ring in the MCLS/GO sheet has a π electron orbital which is perpendicular to the surface of MCLS/GO, so organic molecules with $\text{C}=\text{C}$ and benzene rings could form π - π bond with MCLS/GO.³⁷ From the results that show the migration of characteristic bands and the chemical structure of MB, we could speculate that the adsorption of MB also involves π - π stacking interactions. In addition, the emergence of a new peak at 1329 cm^{-1} and the overwhelming of that at 1386 cm^{-1} originate from the $\text{C}-\text{N}$ stretching vibrations of MB at 1319 and 1389 cm^{-1} , which testify the existence of hydrogen bonding between the hydroxyl of MCLS/GO and the nitrogen of MB.³⁸ The probable adsorption mechanism of MB by MCLS/GO is schematically represented in Fig. 9.

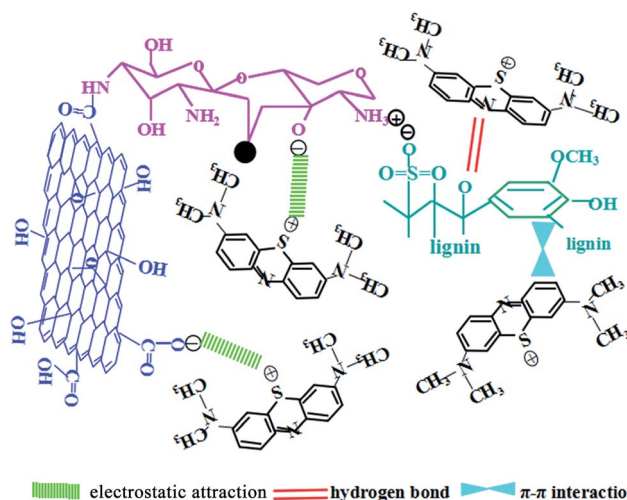


Fig. 9 Schematic illustration of the mechanism of MB adsorption by MCLS/GO.

4. Conclusions

The characteristic results of SEM, XRD, VSM, FTIR, XPS, and zeta-potential indicate that a MCLS/GO composite was successfully prepared. This study clearly demonstrates that MCLS/GO can be utilized as a potential adsorbent for decontaminating MB. MB adsorption characteristics were affected by the surrounding conditions, such as pH, ionic strength and temperature. The adsorption process was well described by a Langmuir model and pseudo-second-order model. The maximum adsorption capacity with addition of 50 mg L⁻¹ SDBS was significantly higher than that of the system without SDBS. The endothermic and spontaneous nature of MB adsorption by MCLS/GO was confirmed by a thermodynamic study. The FTIR spectrum of MCLS/GO before and after adsorption implied that MB was successfully combined with the adsorbents and the adsorption mechanism included electronic attraction, π - π stacking interactions, and hydrogen bonding. Thus, MCLS/GO is a very suitable adsorbent for MB removal from wastewater due to its efficient and fast adsorption behavior, as well as its convenient separation characteristics by an external magnet.

Acknowledgements

This work was supported by the National Science Foundation of China (Grant No. 41271332, 51478470 and 51521006).

References

- 1 F. Khodam, Z. Rezvani and A. R. Amani-Ghadim, *J. Ind. Eng. Chem.*, 2015, **21**, 1286–1294.
- 2 E. Franciscon, D. Mendonça, S. Seber, D. A. Morales, G. J. Zocolo, M. B. Zanoni, M. J. Grossman, L. R. Durrant, H. S. Freeman and G. A. Umbuzeiro, *Process Biochem.*, 2015, **50**, 816–825.
- 3 D. Morshedi, Z. Mohammadi, M. M. Akbar Boojar and F. Aliakbari, *Colloids Surf., B*, 2013, **112**, 245–254.
- 4 C. Wang, Y. Zhang, L. Yu, Z. Zhang and H. Sun, *J. Hazard. Mater.*, 2013, **260**, 851–859.
- 5 M. Peydayesh and A. Rahbar-Kelishami, *J. Ind. Eng. Chem.*, 2015, **21**, 1014–1019.
- 6 L. Liu, B. Zhang, Y. Zhang, Y. He, L. Huang, S. Tan and X. Cai, *J. Chem. Eng. Data*, 2015, **60**, 1270–1278.
- 7 G. L. Dotto, J. M. Santos, I. L. Rodrigues, R. Rosa, F. A. Pavan and E. C. Lima, *J. Colloid Interface Sci.*, 2015, **446**, 133–140.
- 8 H. Saygılı, F. Güzel and Y. Önal, *J. Cleaner Prod.*, 2015, **93**, 84–93.
- 9 J. Gong, J. Liu, Z. Jiang, X. Wen, E. Mijowska, T. Tang and X. Chen, *J. Colloid Interface Sci.*, 2015, **445**, 195–204.
- 10 L. Shi, G. Zhang, D. Wei, T. Yan, X. Xue, S. Shi and Q. Wei, *J. Mol. Liq.*, 2014, **198**, 334–340.
- 11 Y. Shen, Q. Fang and B. Chen, *Environ. Sci. Technol.*, 2015, **49**, 67–84.
- 12 C. J. Madarang, H. Y. Kim, G. Gao, N. Wang, J. Zhu, H. Feng, M. Gorrington, M. L. Kasner and S. Hou, *ACS Appl. Mater. Interfaces*, 2012, **4**, 1186–1193.
- 13 H. Y. Zhu, Y. Q. Fu, R. Jiang, J. Yao, L. Xiao and G. M. Zeng, *Bioresour. Technol.*, 2012, **105**, 24–30.
- 14 L. Fan, C. Luo, M. Sun, X. Li and H. Qiu, *Colloids Surf., B*, 2013, **103**, 523–529.
- 15 L. Fan, C. Luo, X. Li, F. Lu, H. Qiu and M. Sun, *J. Hazard. Mater.*, 2012, **215–216**, 272–279.
- 16 Q. Lü, C. Wang and X. Cheng, *Microchim. Acta*, 2010, **169**, 233–239.
- 17 X.-j. Hu, Y.-g. Liu, H. Wang, A.-w. Chen, G.-m. Zeng, S.-m. Liu, Y.-m. Guo, X. Hu, T.-t. Li, Y.-q. Wang, L. Zhou and S.-h. Liu, *Sep. Purif. Technol.*, 2013, **108**, 189–195.
- 18 X. J. Hu, J. S. Wang, Y. G. Liu, X. Li, G. M. Zeng, Z. L. Bao, X. X. Zeng, A. W. Chen and F. Long, *J. Hazard. Mater.*, 2011, **185**, 306–314.
- 19 D. Depan, B. Girase, J. S. Shah and R. D. Misra, *Acta Biomater.*, 2011, **7**, 3432–3445.
- 20 A. Ye, W. Fan, Q. Zhang, W. Deng and Y. Wang, *Catal. Sci. Technol.*, 2012, **2**, 969–978.
- 21 L. Li, L. Fan, M. Sun, H. Qiu, X. Li, H. Duan and C. Luo, *Colloids Surf., B*, 2013, **107**, 76–83.
- 22 C. Cao, L. Xiao, C. Chen, X. Shi, Q. Cao and L. Gao, *Powder Technol.*, 2014, **260**, 90–97.
- 23 L. Fan, C. Luo, M. Sun, X. Li, F. Lu and H. Qiu, *Bioresour. Technol.*, 2012, **114**, 703–706.
- 24 J. Yang, J.-X. Wu, Q.-F. Lü and T.-T. Lin, *ACS Sustainable Chem. Eng.*, 2014, **2**, 1203–1211.
- 25 S. Luo, X. Xu, G. Zhou, C. Liu, Y. Tang and Y. Liu, *J. Hazard. Mater.*, 2014, **274**, 145–155.
- 26 H. Wang, X. Yuan, Y. Wu, H. Huang, G. Zeng, Y. Liu, X. Wang, N. Lin and Y. Qi, *Appl. Surf. Sci.*, 2013, **279**, 432–440.
- 27 C. Gan, Y. Liu, X. Tan, S. Wang, G. Zeng, B. Zheng, T. Li, Z. Jiang and W. Liu, *RSC Adv.*, 2015, **5**, 35107–35115.
- 28 K. Yang, L. Zhu and B. Xing, *Environ. Pollut.*, 2007, **145**, 571–576.
- 29 J. Li, S. Chen, G. Sheng, J. Hu, X. Tan and X. Wang, *Chem. Eng. J.*, 2011, **166**, 551–558.
- 30 L. Ai, C. Zhang and Z. Chen, *J. Hazard. Mater.*, 2011, **192**, 1515–1524.
- 31 L. Fan, C. Luo, M. Sun, H. Qiu and X. Li, *Colloids Surf., B*, 2013, **103**, 601–607.
- 32 T. Liu, Y. Li, Q. Du, J. Sun, Y. Jiao, G. Yang, Z. Wang, Y. Xia, W. Zhang, K. Wang, H. Zhu and D. Wu, *Colloids Surf., B*, 2012, **90**, 197–203.
- 33 X.-j. Hu, Y.-g. Liu, H. Wang, G.-m. Zeng, X. Hu, Y.-m. Guo, T.-t. Li, A.-w. Chen, L.-h. Jiang and F.-y. Guo, *Chem. Eng. Res. Des.*, 2015, **93**, 675–683.
- 34 T. K. Sen and D. Gomez, *Desalination*, 2011, **267**, 286–294.
- 35 Y. Wang, L. Zeng, X. Ren, H. Song and A. Wang, *J. Environ. Sci.*, 2010, **22**, 7–14.
- 36 X. J. Hu, Y. G. Liu, G. M. Zeng, S. H. You, H. Wang, X. Hu, Y. M. Guo, X. F. Tan and F. Y. Guo, *J. Colloid Interface Sci.*, 2014, **435**, 138–144.
- 37 Z. Wu, L. Zhang, Q. Guan, P. Ning and D. Ye, *Chem. Eng. J.*, 2014, **258**, 77–84.
- 38 Y. Liu, J. Wang, Y. Zheng and A. Wang, *Chem. Eng. J.*, 2012, **184**, 248–255.